Research Article

Glycerol Acetylation with Propionic Acid Using Iron and Cobalt Oxides in Al-MCM-41 Catalysts

Fábio R. Tentor[1], Diego B. Dias[1], Mateus R. Gomes[1], João Guilherme P. Vicente[2], Lúcio Cardozo-Filho[3], Márcio E. Berezuk[1],*

[1]*Department of Chemical Engineering, Federal University of Technology – Paraná, Apucarana 86812460, Paraná, Brazil.*
[2]*FACENS University Center, Sorocaba 18085784, São Paulo, Brazil.*
[3]*Department of Chemical Engineering, State University of Maringá, Maringá 87020900, Paraná, Brazil.*

Abstract

In this work, Al-MCM-41 molecular sieves were synthesized, containing iron and/or cobalt oxides, impregnated by incipient wetness method, characterized and applied as catalysts in the acetylation reaction of glycerol with propionic acid to produce green glyceryl propionate molecules of high commercial value. According to this, X-ray Diffraction (XRD), X-ray Fluorescence (XRF), Fourier Transform Infra Red (FT-IR), adsorption/desorption N_2 isotherms, textural analysis, and Scanning Electron Microscope (SEM) analysis were recorded to evaluate the main characteristics of materials. The presence of Lewis and Brønsted acidic sites and catalysts surface area were observed as important key points to functionalize acetylation reaction. Thus, time reaction, temperature, and glycerol / propionic acid ratio varied to improve the most suitable reaction conditions and behaviors. As a result, glycerol conversion was above 96%, followed by 68% of selectivity to glyceryl monopropionate as well as the formation of glyceryl di- and tri- propionate and a small amount of ethylene glycol dipropionate as an undesired product. Copyright © 2020 BCREC Group. All rights reserved

Keywords: Glycerol; propionic acid; acetylation; Al-MCM-41; iron; cobalt

How to Cite: Tentor, F.R., Dias, D.B., Gomes, M.R., Vicente, J.G.P., Cardozo-Filho, L., Berezuk, M.E. (2020). Glycerol Acetylation with Propionic Acid Using Iron and Cobalt Oxides in Al-MCM-41 Catalysts. *Bulletin of Chemical Reaction Engineering & Catalysis*, 15 (3), 829-844 (doi:10.9767/bcrec.15.3.9020.829-844)

Permalink/DOI: https://doi.org/10.9767/bcrec.15.3.9020.829-844

1. Introduction

Over the last decade, biodiesel has been suggested as a reliable renewable alternative for diesel fossil fuel; mainly due to reduced toxicity, exhaust emissions and enhancing positive carbon cycle for reduction of greenhouse gases.

Therefore, reducing global climate change and global warming [1]. Biodiesel is produced from triglycerides by transesterification with short chain alcohols and a huge amount of glycerol, ca. 10 wt% of the overall biodiesel production, is generated as the by-product in the process [2–4].

Glycerol is one of the most important and promising bioderived platform chemicals from biomass and the major waste byproduct of biodiesel industry [5,6]. Glycerol (or glycerin) has

---

* Corresponding Author.
  Email: berezuk@utfpr.edu.br (M.E. Berezuk);
  Tel/Fax: +554331621200

great application in cosmetics, personal hygiene, food, medicine, and tobacco sectors [7]. In terms of chemical transformation, it still presents limited applications, the main ones on explosives production, like nitroglycerin, and in the formation of alkyd resins [8]. There is a strong motivation to produce fuels from oxygenated molecules generated from biomass conversion [9,10].

Etherification reaction with alcohols, ketones, aldehydes or carboxylic acids are an important way to change glycerol molecule and promote the formation of chemical compounds that present better commercial and economic value, such as renewable fuels additives, surfactants, flavorings and solvents for use in medicine as well as anti-bacterial agents [11–15].

Functionalizing of glycerol with carboxylic acid, acetic acid or propionic acid, for example, produce glycerol esters that have been identified as valuable replacement of fuel additives that are related to depleted sources, price uncertainty and environmental concern of petroleum feedstock [9]. Mono-, di- and tri-acetyl glycerides (MAG, DAG, and TAG) are the main products from the acetylation/propylation of glycerol with acetic or propionic acids and application to fuel additives to improve cold flow, reduce viscosity in biodiesel use and antiknock additives of gasoline [9,13]. Moreover, these glycerol derived products are important building blocks of greener polyester for biorefinery industry [16].

Several studies have been published related to glycerol acetylation with acetic acid using heterogeneous catalysts that enrich both Brønsted and Lewis acidic sites. Acid zeolites, acid clays, modified molecular sieves, heteropoly acids, metal oxides, ion exchange resins, among others, with modifications in their chemical structures, are being responsible for increasing the number of acidic sites that were employed in the production of acetyl glycerides [17–26]. Heterogeneous acidic catalysts showed gains in glycerol functionalization towards derived products. Possibilities of better separation stages, reuse of catalysts or regeneration presents advanced to macroscale process in industry [11,27].

According to Trifoi *et al.* [28], industrial catalysts must have special requirements to the catalyst's projects, for example, it's not recommended to be very sensitive to poisoning and impurities, it's important to allow a huge capacity of production, get cheap structures and metals, have thermal and mechanical resistance and be recyclable. MCM-41 molecular sieves present all those characteristics, related to applications in industry, and not only added the possibility to incorporate trivalent atoms (Al, Fe, Ga) but also other transition metals (Sn, Zn, Ir) in the porous / walls of the MCM-41 that promotes Lewis and Brønsted acidic sites environment functionalizing reaction mechanisms and improving selectivity and yields [8,29–34].

Some papers have highlighted the application of iron and cobalt oxides supported on zeolites or molecular sieves in the acetalization or acetylation of glycerol [21,35–36]. These metals were able to modify and promote glycerol functionalization in esters of great commercial value.

The large number of published works related the use of acetic acid in glycerol acetylation contrasts with small number of studies using propionic acid in reactions of glycerol propylation. This fact opens more horizons for scientific research. The oldest works found dated from the 1930s with homogeneous catalysis in obtaining mono-, di- and tri-propyl glycerides [37–38]. Cho *et al.* [39] carried out reactions for glycerol transformation with different dicarboxylic acids to obtain esters derived from glycerol. Rathod and collaborators [40] studied the esterification of propionic acid with isopropyl alcohol, observing feasibility in the production of its derived esters. Recently, Saengarum *et al.* [41] published scientific work which studied the glycerol propylation with propylene and 1-butene hydrocarbons to obtain mono-, di- and tripropyl glycerol ethers to use as fuel additives. Commercial acid resins were employed as catalysts, corroborating that acid catalysis favored an increase in reaction yield.

Acidic routes favored acetylation glycerol reactions mostly by the use of acetic acid but rare published information presented glycerol acetylation with propionic acid, which characteristics could improve new green molecules. Iron and cobalt oxides present themselves as materials with a great acid capacity according to Pearson's theory of hard and soft acids, and this acid capacity of these metals has been little explored in the glycerol transformation.

In this context, our studies present novelty in perform acetylation reactions of glycerol with propionic acid, an important underexplored molecule to form mono-, di-, and tripropyl glycerides (MPG, DPG, and TPG). Our proposal is to functionalize this reaction with catalysts containing acidic characteristics promoted by Al-MCM-41 containing iron and cobalt oxides applied to improve glycerol chemistry transformations.

2. Materials and Method

2.1 Materials

Glycerol (99%, Synth Inc., Brazil), propionic acid (99%, Vetec Chemical Inc., Brazil), methanol (99.5%, Dinâmica Chemical Inc., Brazil), sodium chloride and sodium hydroxide (Vetec Chemical Inc., Brazil), sodium metasilicate pentahydrate and aluminum sulfate hydrate (99%, Êxodo Scientific Inc., Brazil), cobalt(II) nitrate hexahydrate (99%, Dinâmica Chemical Inc., Brazil), iron(III) nitrate nonahydrate (99%, Vetec Chemical Inc., Brazil), cetyl trimethyl ammonium bromide (CTAB, 99%, Sigma-Aldrich, US) and sulfuric acid (95-98%, Hexis Scientific, Brazil) are from an analytical standard used without prior treatment. Monoethylene glycol (99%, Vetec Chemical Inc., Brazil) was used as an internal standard for gas chromatography (GC) analyses. Magnetic and mechanic stirrer with heating control, pH meter and a variety of different glassware were also used.

2.2 Preparation of Catalysts

Al-MCM-41 template structure was prepared by sol-gel method described by Heravi *et al.* [31] and Preethi *et al.* [42] with modifications. Molecular sieves molar compositions defined for the catalysts template were $SiO_2:xAl_2O_3:0.2CTAB:0.89H_2SO_4:120H_2O$ which results in two different Al/Si ratios 1/5 and 1/25.

Briefly, sodium metasilicate (38 g) and aluminum sulfate (11.25 g and 2.25 g) were dissolved in a beaker with distilled water in magnetic stirrer for 1 h. Aluminum solution was slowly mixed with silicon solution and stirred by 30 minutes to homogenize. Sulfuric acid solution was added to mother liquor solution drop by drop until reach pH 10.5 resulting in a gel texture appearance in the solution. After pH adjustment, CTAB solution was prepared and added slowly to the gel mixture with mechanic stirrer keeping it in movement by an hour. The gel material formed was transferred to Teflon-coated autoclaves vessels to age the solution and kept in an air-drying lab oven at 145 °C for 40 hours. Then the solid product obtained was filtered, washed several times with distilled water and dried at 95 °C in an air-drying oven for 2 h. Then the sample was calcined in a muffle furnace at 550 °C for 15 h (0.7 °C.min⁻¹ ramp rate) to remove the template.

To maximize Brønsted acidic sites in Al-MCM-41 an ion exchange procedure was done mixing the obtained white powder with a solution of ammonium chlorate (1 M), twice times. This mixture was kept in magnetic stirring for 24 hours in room temperature. Solution was filtered, dried and calcined again at 550 °C for 4 h in air atmosphere.

Iron and/or cobalt metals were added to Al-MCM-41 materials by incipient wetness impregnation method described by Decyk *et al.* [43]. After determining the apparent volume of the Al-MCM-41 in a graduate beaker, a volume 10 times greater were used to prepare the solution. Iron(III) nitrate hexahydrate and/or cobalt(II) nitrate nonahydrate were dissolved in distillate water to provide 10 wt% total metal in catalysts. The solution was kept in magnetic stirrer for 1 hour and then the material temperature was raised to 70 °C for a period of 6 hours, until the material dried. After material was dried at 95 °C in an air-drying oven for 3 h and calcined in a muffle furnace at 550 °C for 4 h. Six different catalysts were able to test which codes were named Fe5, Fe25, Co5, Co25, FeCo5, and FeCo25.

2.3 Products Analysis

Analysis of the reaction products identified the Shimadzu QP-2010 Ultra gas chromatography with mass detector (GC-MS), using Rtx-Wax (Restek) column with 30 m × 0.25 mm × 0.25 μm. The temperature of the injector chamber was 250 °C, varying the oven temperature from 40 °C to 200 °C with a rate of 10 °C.min⁻¹ with hold for 9 minutes in final temperature. Split dilution was used at 1:60. External standard for GC analysis was used for the quantification of glycerol and benzaldehyde. The monoethylene glycol was used as internal standard diluted on methanol in the concentration of 100 mg.mL⁻¹, to products quantification.

Glycerol conversion calculations, as well as the selectivity for desired products and the final reaction yield are defined by Equations 1 to 3 [44].

$$Conversion\ (\%) = 100 \times \frac{(initial\ mols\ reagent - final\ mols\ reagent)}{initial\ mols\ reagent} \tag{1}$$

$$Selectivity\ (\%) = 100 \times \frac{desired\ mols\ product}{(initial\ mols\ reagent - final\ mols\ reagent)} \tag{2}$$

$$Yield\ (\%) = \frac{Conversion\ (\%) \times Selectivity\ (\%)}{100} \tag{3}$$

2.4 Reactional Experiments

The experiment was conducted through etherification of glycerol with propionic acid in 50 ml borosilicate glass batch sealed reactors, without use of organic solvents. Moreover, to control the reaction solution, external-controlled hotplates with external thermostat and a magnetic vigorous stirring system were used to avoid or diminish mass and heat transfers resistances. Besides that, the reactor was not attached to the reflux condenser in order to remove excess water from the reaction solution.

In a typical reaction procedure, 25 mmol of glycerol (2.3 g) was added with 125 mmol of propionic acid (9.26 g) (related to 1/5 glycerol / acid ratio). The use of 100 mg of catalyst per test was fixed and the reaction time varied from 2 to 4 hours. Besides that, five temperatures ranging from 90 °C until 140 °C, and the ratio of glycerol to propionic acid were observed always with acid excess in reaction medium. At the end of the reactions, an amount of material was filtered on qualitative filter papers (grade 4) with cotton, collected in 2 mL vials and stored in a freezer. All experiments were performed in duplicate form. Reaction conditions exploited was chosen according to literature researches [12,45].

2.5 Instrumentation

The X-ray diffraction (XRD) patterns of molecular sieves synthesized catalysts were obtained by using a Bruker powder diffractometer D2 PHASER model using Cu-Kα radiation, nickel filter, 10 mA and 30 kV in the high voltage source, and scanning angle between 10° and 70° of 2θ with 0.02° steps per second. Adsorption/desorption experiments using N_2 were carried out at 77 K on a Quantachrome NOVA 1200 instrument. Before each measurement the samples were first outgassed at 423 K for 12 h at 5×10^{-3} Torr and then at room temperature for 2 h at 1×10^{-5} Torr. The N_2 isotherms were used to determine the specific surface areas, pore volume, and pore diameter using the BET equation and BJH theory. Infrared spectra were collected on a FTIR Bruker model Vertex 70 spectrophotometer, with KBr as dispersant and the spectra was recorded from 400 cm^{-1} to 4000 cm^{-1} with a resolution of 4 cm^{-1} and total of 10 scans. X-ray Fluorescence spectroscopy (XRF) analysis was recorded by Rigaku Supermini 200 using Pd X-ray tube with 50 kV voltage and 4mA. Catalysts were also characterized using scanning electron microscopy (SEM) with a Shimadzu scanning electron microscope model SSX-550 Superscan with an accelerating voltage of 30 kV and different magnifications.
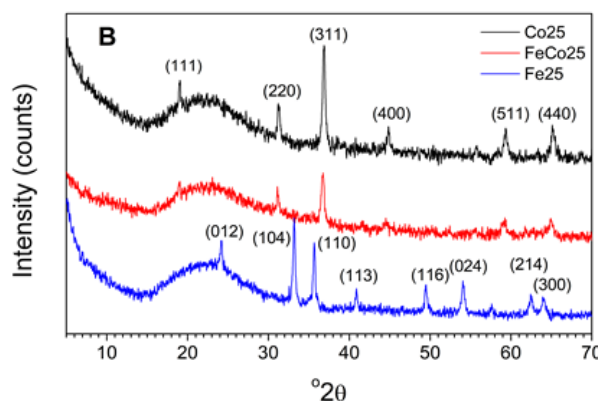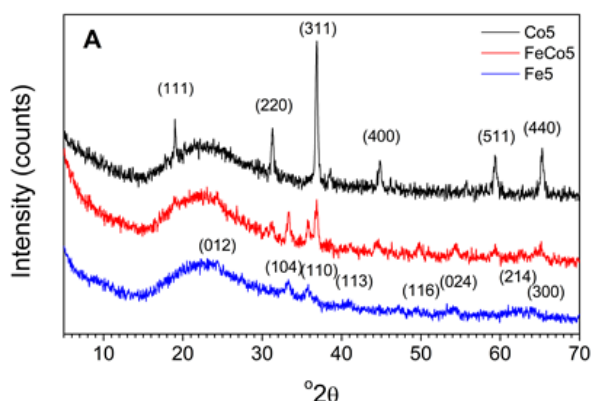
3. Results and Discussion

3.1 Characterization

X-ray diffraction patterns of calcined mesoporous Al-MCM-41 precursors and Fe/Co-Al-MCM-41 catalysts samples are shown in Figure 1 and 2. At low angle X-ray diffraction pat-
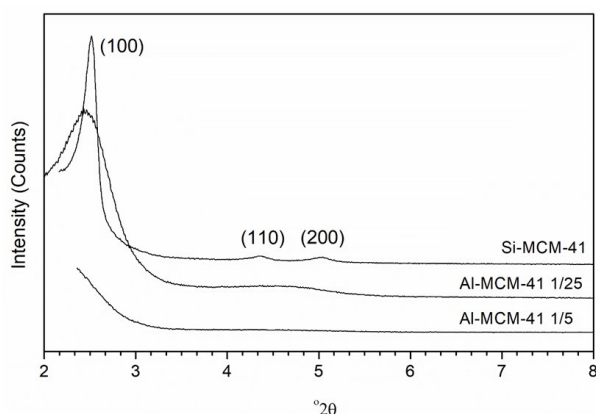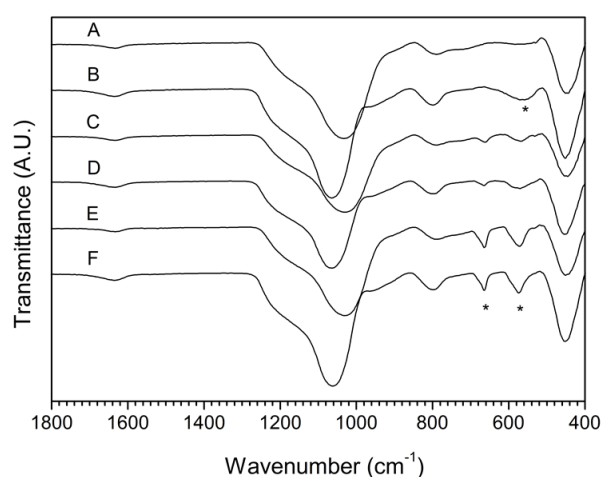

Figure 1. Low angle XRD patterns for catalyst precursors.

Figure 2. XRD patterns of the Sn-Al-MCM-41 catalysts samples in the domain of 10-70 (2θ).

terns exhibit typical MCM-41 signs with strong peak in the 2θ range of 2-3–2.6° due to (100) reflection lines but as larger amounts of aluminum are present in the structure this (100) reflection present peaks going broader and less intense. High Al content in MCM-41 contributes to diminish orderly the structural pore channels and the main intense peak shifts towards higher interplanar spacing and this behavior represents an increase in the pore size of the MCM-41 material [46–47,59]. This modified interplanar spacing can be explained about of replacement of shorter Si–O bonds (1.60 Å) by longer A1–O bonds (1.75 Å) in the MCM-41 structure [59]. Other Miller´s indices (110) and (200) also presents same behavior and the well-defined peaks disappears to form a broad peak

in Si/Al in 1/25 and totally disappears in 1/5. The d_{100} spacing, lattice parameter (a_0), and Scherrer calculated values are presented in Table 1.

In Figure 2, a typical iron(III) oxide (Fe_2O_3) and cobalt(II,III) oxides ($CoO.Co_2O_3 \rightarrow Co_3O_4$) diffractogram peak patterns from Fe/Co-Al-MCM-41 samples are observed by the Miller indices. Spinel phase of cubic Co_3O_4 crystalline cell patterns are presented in the all cobalt synthesized catalysts and hematite hexagonal Fe_2O_3 crystalline cell patterns are showed in all iron synthesized catalysts [48–49]. No other phases/shift in peak positions were observed by XRD in this study which suggests that no extensive solid solution was formed between the two oxides as a result of this preparation catalyst impregnation method.

Iron and cobalt oxides presented different crystallite dimensions calculated by Scherrer equation [50–51], while Co_3O_4 crystals showed increased dimensions if compared with Fe_2O_3 crystals (Table 1). This behavior is repeated even when the concentration of iron and cobalt elements are reduced by half in the catalysts FeCo5 and FeCo25. Unfortunately, no iron signal can be seen on FeCo25 sample patterns.

Figure 3 reports the FT-IR spectra for all Fe and Co synthesized catalysts in 1800–400 cm^{-1} range. In all sample's curves, the band in 1640 cm^{-1} correspond to the $\upsilon_{O–H}$ vibrations of silanol groups [52], while strong bands around 1230 and 1060 cm^{-1} correspond to $\upsilon_{\equiv Si–O–Si\equiv}$ and $\upsilon_{Si–O–Si}$ asymmetric stretching, typical for MCM-41. Curves A, C and E, which correspond to Fe5, FeCo5 and Co5 catalyst, have a structure with higher Al content, then this behavior

Figure 3. FT-IR spectra for synthesized catalysts. A) Fe5, B) Fe25, C) FeCo5, D) FeCo25, E) Co5 and F) Co25.

Table 1. Textural analysis and metal loading percentage.

Materials	Si/Al	Angle (°2θ)[a]	d_{100} (Å)[b]	a_0 (Å)[c]	D_{sc} (Å)[e]
Si-MCM-41	-	2.5	35.0	40.1	-
Al-MCM-41	1/5	2.3	38.7	44.7	-
Al-MCM-41	1/25	2.4	36.3	41.9	-
Fe5[d]	1/5	33.2	2.7	2.2	36
Fe25[d]	1/25	33.2	2.7	2.2	71
Co5[d]	1/5	36.9	2.4	2.0	108
Co25[d]	1/25	36.9	2.4	2.0	108
FeCo5[d]	1/5	33.4 / 36.9	2.7 / 2.4	2.2 / 2.0	53 / 86
FeCo25[d]	1/25	- / 36.9	- / 2.4	- / 2.0	- / 48

[a] Miller index (100) for molecular sieves precursors, (104) for Fe catalysts and (311) for Co catalysts.
[b] Interplanar spacing parameter.
[c] Lattice crystal parameter: $a_0 = 2d_{100}/3^{0.5}$.
[d] Parameters referring to the Fe_2O_3 and Co_3O_4 crystals.
[e] Mean size diameter for crystallites Fe_2O_3 and Co_3O_4 sites by Scherrer Equation calculation [51].

shifts in approximately 30 cm^{-1} (1060–1030 cm^{-1}) the siloxane bands, this shifting band occurs due to SiO$_4$ and AlO$_4$ tetrahedral simultaneous vibrations [53]. The band around 970 cm^{-1} correspond to a vibration mode of SiO$_4$ perturbed by the presence of neighboring Fe$_2$O$_3$/Co$_3$O$_4$ or Fe=O (OH) / Co=O (OH) group. The presence of this band is attributed to the formation of $\upsilon_{Si–O–Si}$ linkages in metallosilicates [54]. Symmetric vibrations $\upsilon_{Si–O–Si}$ signs appear near 800 cm^{-1}. The band at 450 cm^{-1} may be assigned to $\upsilon_{Si–O}$ tetrahedral vibration [55]. The $\upsilon_{Fe–O–Fe}$ stretching vibration, characteristic of Fe$_2$O$_3$ is observed at approximately 560 cm^{-1} and $\upsilon_{Co–O–Co}$ stretching vibration, characteristic of Co$_3$O$_4$ is observed approximately 573 cm^{-1} and 670 cm^{-1} [56–58].

The results of the chemical analysis of the catalysts are given in the Table 2 and adsorption/desorption isotherms curves are presented in Figure 4. Classic MCM-41 molecular sieves isotherms type IV which represents mesoporosity materials are observed when Al/Si ratio are 1/25 which curves shows a smaller hysteresis behavior due to capillary condensation of N$_2$ in the primary mesopores. Increasing the presence of Al in MCM-41 to provide Al/Si in 1/5 parts disorder the structure modifying interplanar spacing, lattice crystal parameters and had consequences for diminish strongly the surface area and pore volume. The enlargement of the unit cell observed by lattice crystal parameters by the presence of high Al content followed by addition of iron and/or cobalt oxides in the pores structure aimed to these behaviors in MCM-41 [59–61]. Fe5, FeCo5, and Co5 catalysts isotherms clearly shows poor crystallinity compared to Fe25, FeCo25, and Co25 [30,59].
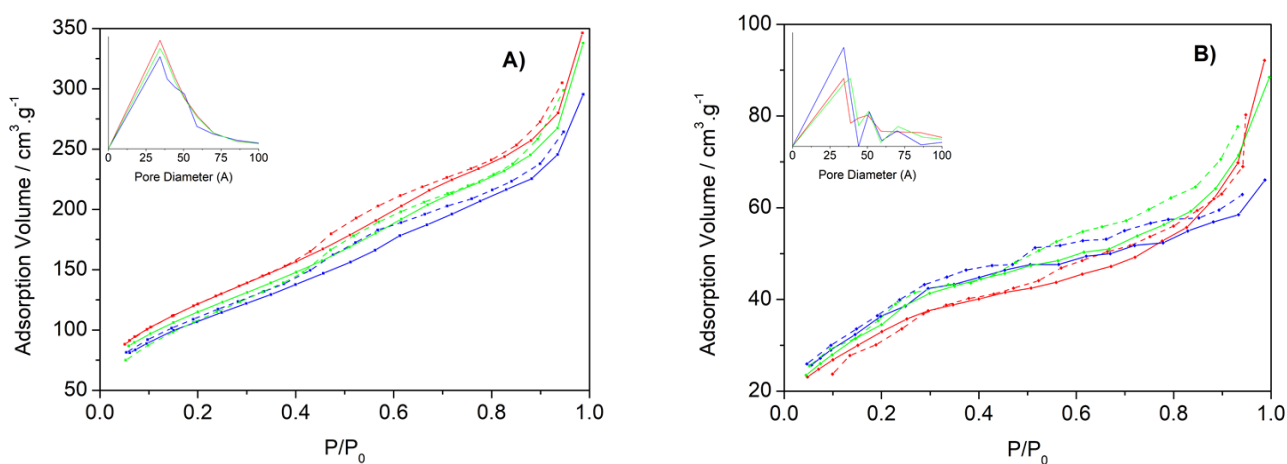
Figure 4. Adsorption / desorption isotherms for the catalysts. A) Al/Si ratio in 1/25 and B) Al/Si ratio in 1/5. Legend: ♦ Fe25 or Fe5, ♦ Co25 or Co5, ♦ FeCo25 or FeCo5. Line and symbol are Adsorption points, Dash and symbol are Desorption points.

**Table 2.** XRD parameters for the synthesized materials.

Catalysts		Fe5	FeCo5	Co5	Fe25	FeCo25	Co25
Surface Area (m^2.g^{-1})	Micro[a]	57	74	95	175	152	162
	Meso and External[a]	63	58	39	261	259	222
	Total[a]	120	132	135	436	411	384
Pore Volume (cm^3.g^{-1})	Micro[a]	0.024	0.031	0.043	0.090	0.074	0.086
	Meso	0.074	0.060	0.058	0.316	0.341	0.250
	Total[b]	0.098	0.091	0.101	0.406	0.415	0.336
Mean Pore Diameter (Å)[b]		34.2	36.3	34.2	34.4	35.6	36.3
Fe Load (%, m/m)[c]		9.65	4.77	-	9.52	4.68	-
Co Load (%, m/m)[c]		-	4.94	10.21	-	4.88	9.75

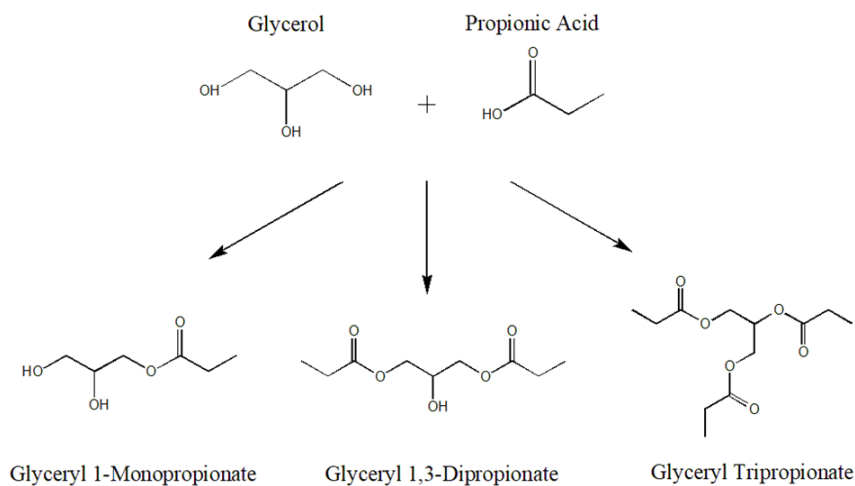[a] The *t*-Plot method were used to obtain micropores e meso-external surface area data.
[b] BJH method were used to determine mean pore diameter and total pore volume.
[c] Metal Fe and Co content were obtained by XRF analysis.
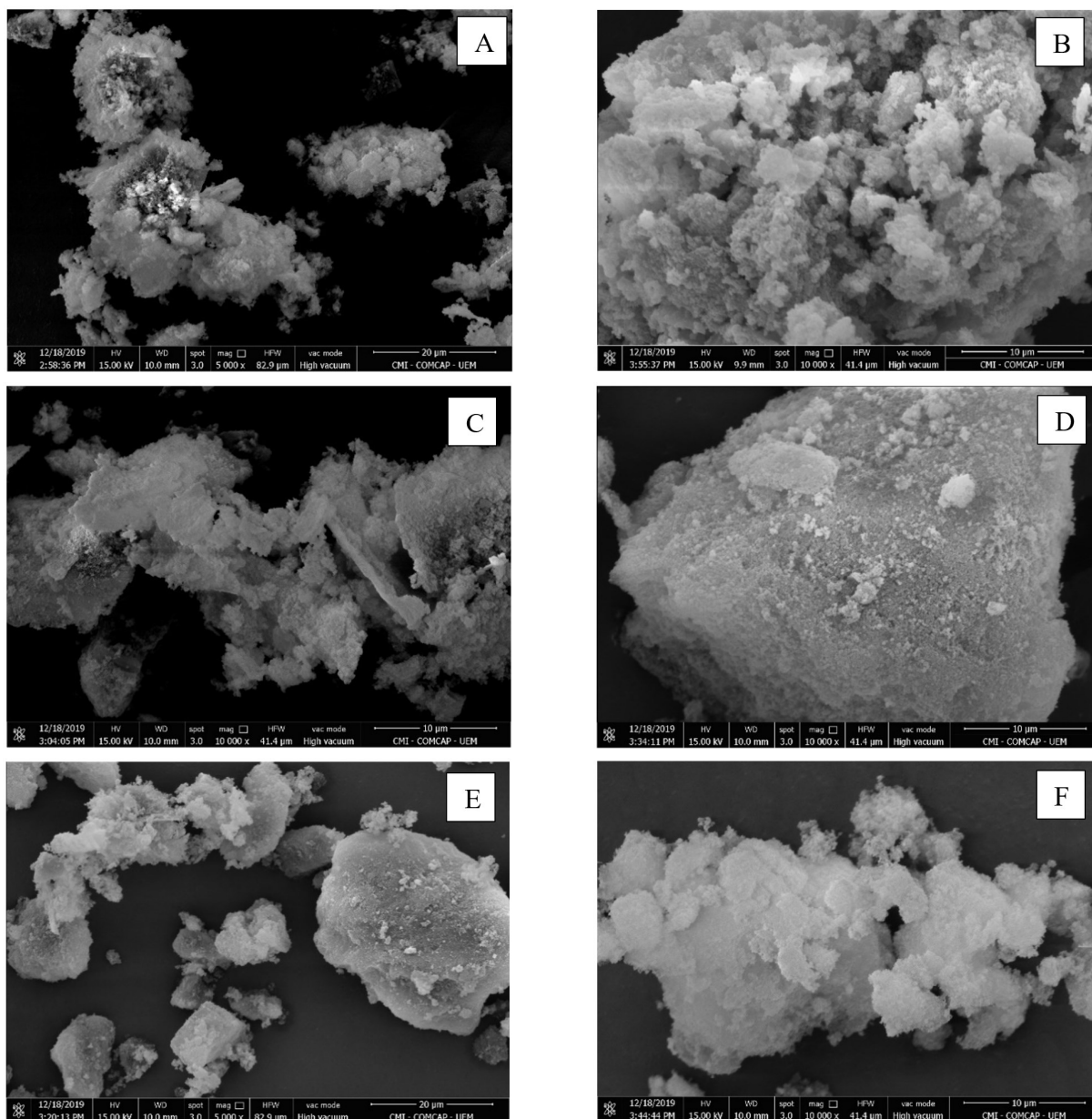
Figure 5. SEM micrographs recorded in 5000x or 10000x images of A) Fe5, B) FeCo5, C) Co5, D) Fe25, E) FeCo25 and F) Co25 catalysts.

Figure 6. Reaction scheme for glycerol acetylation.

Figure 5 shows scanning electronic microscopy images (SEM) for all synthesized catalysts. All catalysts sample presented spherical small crystallites alternating between well-defined structures to greater particle non-uniform clusters. This morphology characteristics is typical for Al-MCM-41 and the more aluminum is inserted into the MCM-41 matrix structure itself, the greater the tendency to observe a more dispersed material containing a less defined morphology [52,62–64].

3.2 Glycerol Etherification Reactions

Fe/Co-Al-MCM-41 catalysts were tested in the etherification reactions of glycerol with propionic acid. We considered the formation of Glyceryl 1-Monopropionate (MPG), Glyceryl 1,3-Dipropionate (DPG), and Glyceryl Tripropionate (TPG) as desired major products, besides that, the formation of Ethylene Glycol Dipropi-

onate as undesired product. Diglycerol also could be formed but no GC-MS signal detected the presence on chromatograms (Figure 6).

In the first stage of experiments, all six catalysts were applied in reactions where the temperature was set at 110 °C, the glycerol/acid ratio was 1/5 (propionic acid excess) and the catalyst mass was 100 mg per test, all in duplicate. Catalysts were evaluated for 2 h and 4 h. Figure 7 and Figure 8 shows the reaction yield in relation to glyceryl 1-monopropionate (MPG) product, in addition to the selectivity for all the products observed.

Catalysts that have both iron oxides and cobalt oxides were shown to be more active compared to catalysts that contain only one of the metal oxides. Catalysts with cobalt oxides have higher conversion values compared to catalysts with iron oxides. Catalysts with a high aluminum content (Al/Si = 1/5) showed lower conversion values compared to catalysts with a lower concentration of this metal in the matrix of MCM-41 (Al/Si = 1/25). The available surface area for catalysis is an important factor for a better reaction performance and this characteristic proved to be more relevant, even with the presence of a higher concentration of aluminum atoms in the framework or extra-framework. The insertion of Al can offer more Lewis acid sites to the catalysts surface and alters the structure of silicates to offer Brønsted sites according to the Löwenstein rule [65–66]. MPG product proved to be the main molecule obtained with selectivity between 78 to 90% and, as the conversion values increase, also does the formation of DPG and TPG, but on a still low scale, up to 15% selectivity for DPG
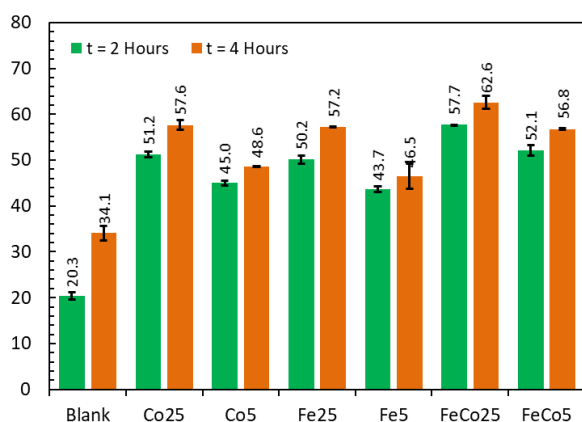
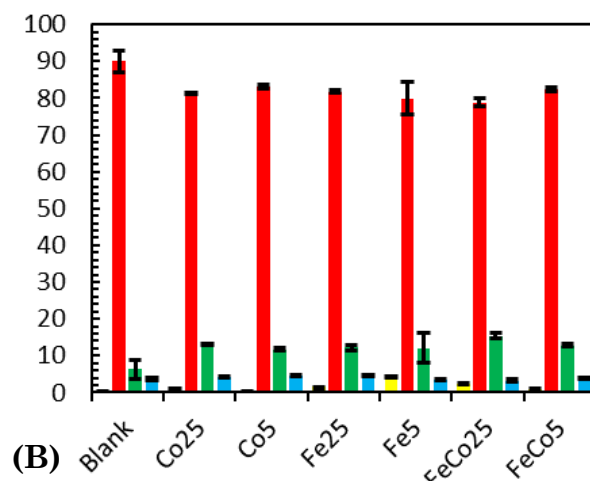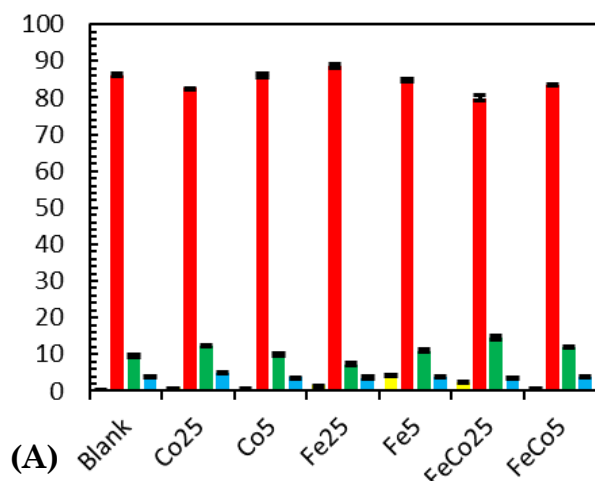**Figure 7.** Reaction yield (%) to MPG product.

Figure 8. Selectivity (%) to all reaction products observed in (A) 2 hours and (B) 4 hours of reaction. Legend: ▪ Glyceryl Tripropionate, ▪ Glyceryl 1-Monopropionate, ▪ Glyceryl 1,3-Dipropionate, ▪ Ethylene Glycol Dipropionate.

and only 5% for TPG. The by-product Ethylene Glycol Dipropionate was also observed in up to 5% selectivity. Despite the lower conversion value, Fe5 catalyst was the only material that favored the formation of TPG, under the conditions presented. It is possible that the more acidic characteristics of the catalyst together with the hard acid dynamics of iron oxide may favor the achievement of TPG. After 4 hours of reaction, yields above 60% were obtained in acetylation of glycerol with propionic acid, at a temperature of only 110 °C, which shows that the use of the molecular sieve Al-MCM-41 containing iron and cobalt is important to functionalize glycerol towards values green products.

It is observed that there is a junction between the catalysts acidic characteristics associated with the surface area availability for chemical contact of the catalysis sites with the reagents (Table 2). The synthesis of Al-MCM-41 and its modification to maximize acidic sites of both Lewis and Brønsted sites are shown to be present in all catalysts. However, the insertion of iron and cobalt metals is the key point for the increase conversion and yields (Figure 7). The concept of acidity provided by transition metals is best explained by the Theory of Hard and Soft Acids by Ralph Pearson [67]. Pearson defined species more polarizable as soft (acid or base) and less polarizable as hard (acid or base). The hardness or softness value can be determined using the values of ionization potential and electronic affinity of these species [68]. XRD analysis showed the presence of Fe^{3+} and Co^{3+}/Co^{2+} in the form of oxides of different nanometric sizes (36–108 Å, Table 1) and the trivalent metals are classified as hard acids (higher acidity index) and the divalent metal as

a characteristic intermediate acid. In this sense, the presence of these metals is strongly beneficial in the glycerol acetylation with propionic acid.
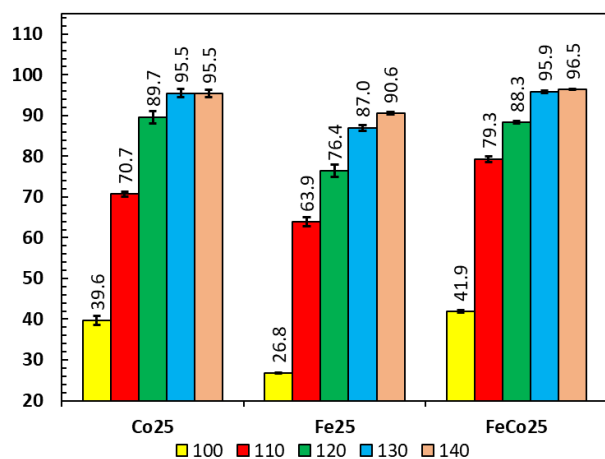
3.3 Temperature Reaction Dependence

In this second stage, the reaction temperature varied, while the other parameters were kept constant, to observe what would be the reaction behavior with increasing temperature. Moreover, only the catalysts that showed the highest reaction yield in the first test stage were used: Fe25, Co25, and FeCo25. It was observed that the reaction depends strongly of the increase of the temperature from 100 °C (Figure 9), and glycerol conversion tends to stabilize close to 95% from 130 °C. In this way, a temperature of 140 °C did not prove to be advantageous for significantly increasing of glycerol conversion values. Catalysts containing cobalt showed to be more active than iron, reaching higher conversion values as the temperature increased.

The maximum MPG yield is reached at 130 °C (approximately 68%) and has a slight decline at 140 °C (Figure 10). Again, a greater formation of TPG (13.1%) occurs with the use of the catalyst containing iron (Fe25), a behavior observed in the first stage of experiments that can be explained by Pearson's theory, previously analyzed.

Zhang *et al*. [36] investigated the use of M-AlPO$_4$ zeolite containing some transition metals, including cobalt, in the acetalization reaction of glycerol with acetone. Even having a behavior of a smaller surface area and lower acidic sites characteristics compared to the best catalyst used, the cobalt containing catalyst proved to be a material capable of offering the second-best reaction yield, under the investigated conditions (yield 67%). This result shows to be important for the use of cobalt as an active site in glycerol acetalization. A similar result was observed for the same reaction using cobalt catalysts in layered double hydroxide (LDH), where a yield of around 70% of reaction was achieved [35].

Gonzales-Arellano *et al*. [21] performed glycerol acetalization with levulinic acid using Zr-SBA-16 containing different Zr levels. At 100 °C and 15 hours of reaction, his best results reached around 70% conversion, 77% selectivity for monoglycerides and 23% for diglycerides. A behavior similar to the data presented in this work. It is worth noting that the appearance of triglycerides occurred at a higher temperature after the conversion approached

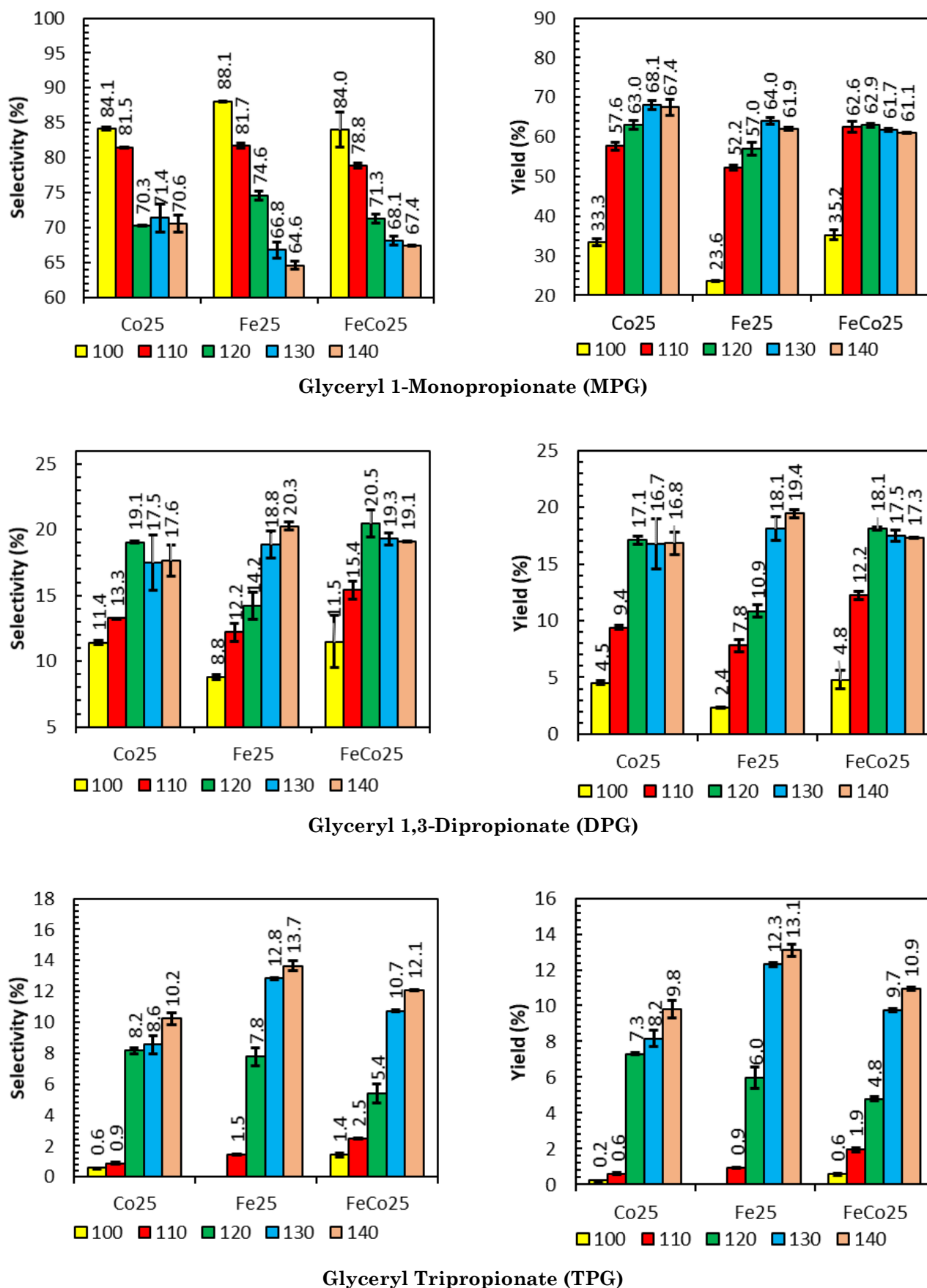**Figure 9.** Glycerol conversion (%) with varying temperature (°C).

Glyceryl 1-Monopropionate (MPG)

Glyceryl 1,3-Dipropionate (DPG)

Glyceryl Tripropionate (TPG)

Figure 10. Selectivity (%) and products yields distribution (%) with varying temperature (°C).

100%, which demonstrates a behavior of occurring consecutive reactions as the glycerol is depleted as a limiting reagent in the process.

Saengarum *et al.* [41] compared Amberlyst-15 resin with commercial sulfated B100 and B200 resins by applying them in the etherification of glycerol with propylene, a molecule of size close to propionic acid. At 100 °C and 8 hours of reaction, only Amberlyst-15 resin was able to convert glycerol into mono-, di-, and triglycerol ethers with 60% conversion. As the reaction time was extended to 16, 24, and 72 hours, the sulfated resins also showed the same products reaching up to 72% conversion. The acid capacity of Amberlyst-15 favored the results obtained, but the deterioration of its molecular structure associated with the formation of coke in its pores significantly reduced its use in sequential reactions.

It is observed with the investigated works and with the experiments carried out (Figure 9 and 10) that as the reaction exhausts glycerol, DPG and TPG tends to appear in greater quantities as the reaction time and increasing temperature. The preference for the formation of the MPG is given by the easier supply of glycerol in the initial stages of reaction. When glycerol is depleting from reaction medium, the excess of propionic acid continues to react with MPG to form DPG and, likewise, to produce TPG. Acidic surface capacity associated with the availability of catalytic sites of the materials, are catalyst highlighted keys in the formation derived products from glycerol and propionic acid.

3.3 Reagents Ratio Dependence

Glycerol acetalization reactions with propionic acid were also carried out by changing the concentrations of reagents, keeping the temperature constant at 110 °C, as well as other
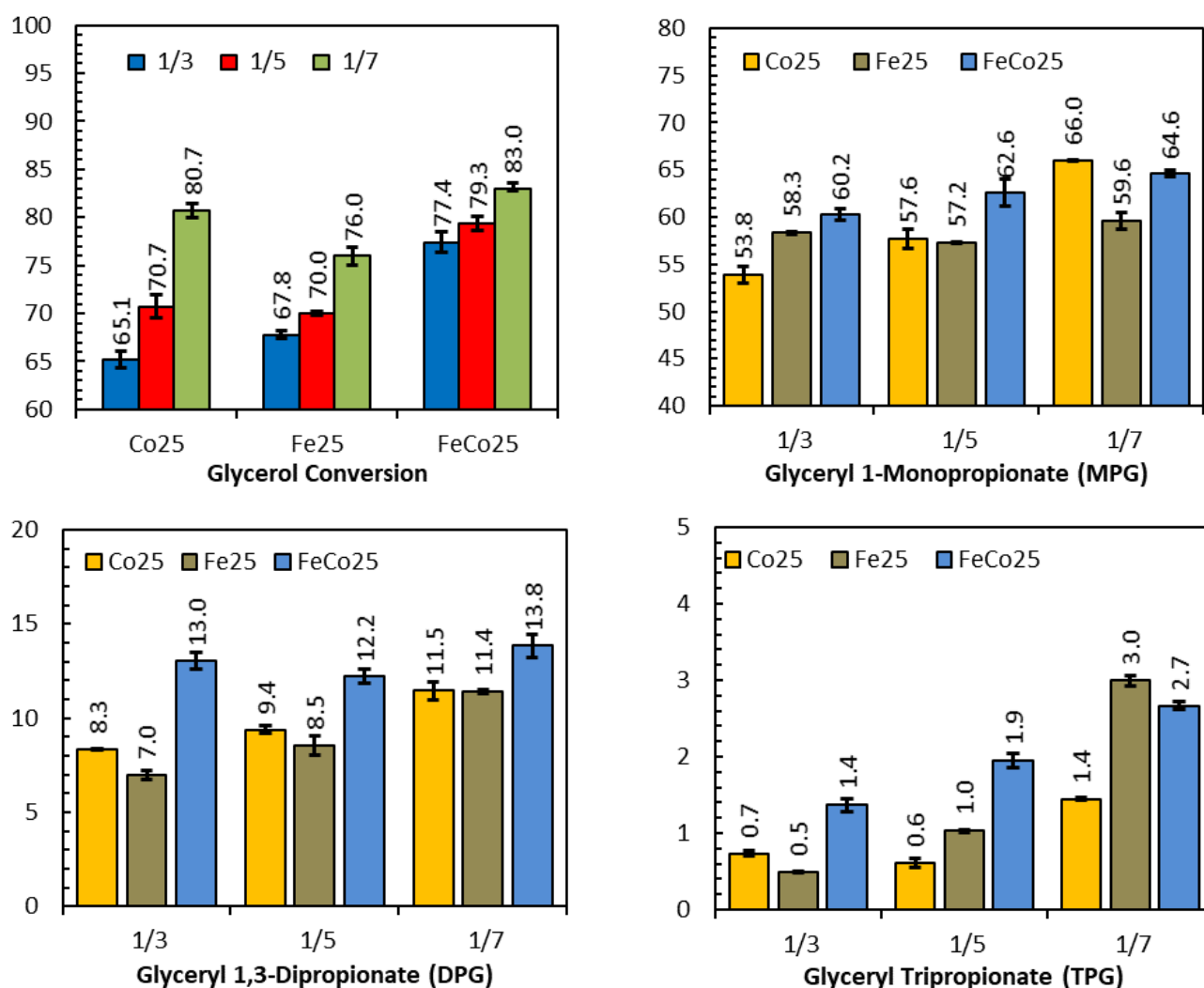
Figure 11. Glycerol conversion (%) and products yields (%) in different glycerol / propionic acid ratios and catalysts.

constant parameters. Reactions containing the excess acidic conditions in the Glycerol / Acid ratio in 1/3, 1/5 and 1/7 were analyzed.

It is noted that the increase in propionic acid concentration shifted the reaction to the products (Figure 11), increasing the glycerol conversion for all catalysts tested and favoring the consecutive reactions to form DPG and TPG. It can also be seen that the Co25 catalyst favored the formation of MPG more, reaching a yield of up to 66% with a corresponding selectivity of 81.8% (Figure 12). Fe25 catalyst was more inclined to form TPG, but was less effective in converting glycerol, which reduced its final yield values. The FeCo25 catalyst proved to be more versatile in forming DPG, but its high conversion was responsible for having the best reaction yield values. As the general characteristics of all catalysts are very close, the differences in selectivity and final reaction yield are also similar. However, all materials tested were capable of transforming glycerol and forming MPG, DPG, and TPG, important green platform molecules capable to improve renewable energy technologies and new products.

4. Conclusions

Synthesis and characterization of Al-MCM-41 molecular sieves, impregnated with iron and/or cobalt, was carried out and applied as catalysts in the glycerol acetylation reaction with propionic acid to the product glyceryl mono-, di-, and tri-propionates. XRD analysis identified Fe_2O_3 and Co_3O_4 oxides with nanometric dimensions and FT-IR showed shift bands by the high presence of aluminum in silicate Al-MCM-41 characteristics and the presence of all structures indicate Lewis and Brønsted acidic sites in the synthesized catalysts. XRF adsorption/desorption N_2 isotherms and textural analysis presented MCM-41 molecular sieves behavior with micropores and mesopores differences according with Al content in the structure and also Fe/Co mass percentage. SEM images showed the presence of spherical small crystallites alternating between well-defined structures until non-uniform clusters. This characteristic view is caused by the high presence of aluminum which increase less defined morphology in MCM-41.

Glycerol acetylation reactions with propionic acid formed mostly glyceryl propionates (mono, di and tri). High yields and selectivity values were obtained in the reactions reaching 79% yield and 90% to MPG selectivity in 110 °C condition. Increasing temperature to 130 °C and the rise of propionic acid concentration
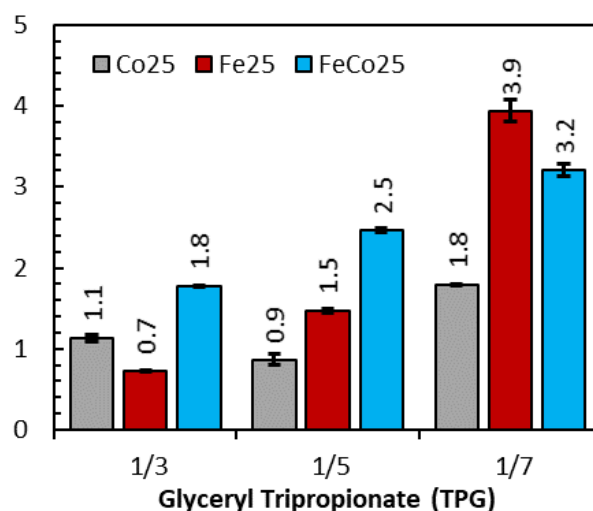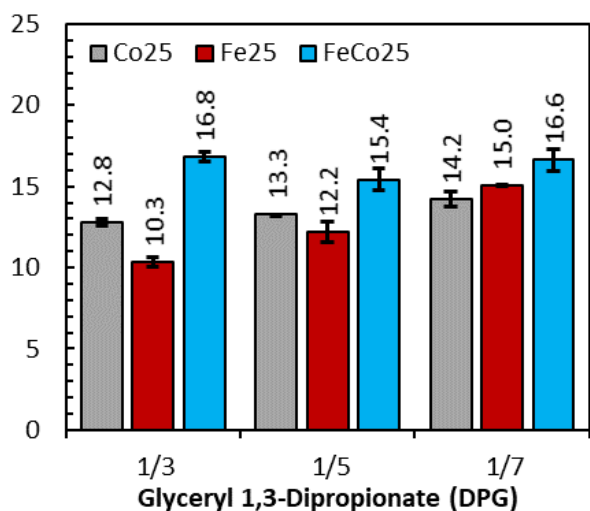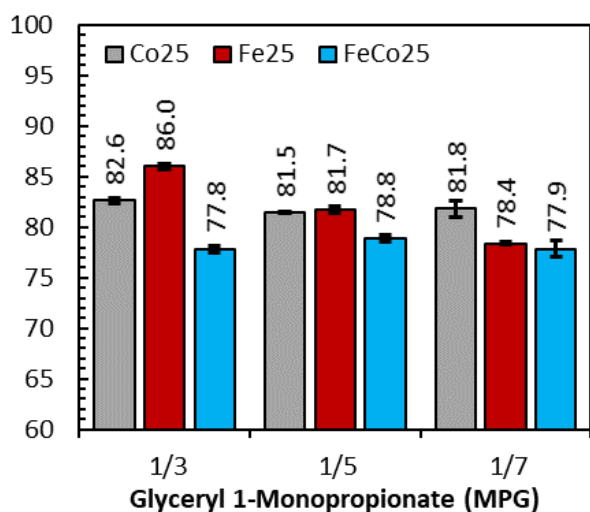
Figure 12. Products selectivity distribution (%) with varying glycerol/propionic acid ratios and catalysts.

were favorable to increase the glycerol conversion up to 95% and maximize selectivity to MPG up to 68%. As the reaction time and temperature advances, the formation of DPG and TPG is observed and, consequently, the decrease of MPG as formed products. In general, catalysts containing iron oxide and a high concentration of aluminum in the chemical structure obtained lower glycerol conversion values, but showed a slightly higher selectivity for DPG and TPG, when compared to catalysts containing cobalt and with lower aluminum content in the structure. The highest reaction yields were obtained with the use of catalysts containing cobalt and iron-cobalt, however more MPG was formed. The acidic materials characteristics associated with the surface area of the pores proved to be determinant for increasing productivity in the formation of glyceryl propionates.

Acknowledgment

References

[1] Faria, R.P.V., Pereira, C.S.M., Silva, V.M.T.M., Loureiro, J.M., Rodrigues, A.E. (2013). Glycerol valorisation as biofuels: Selection of a suitable solvent for an innovative process for the synthesis of GEA. *Chemical Engineering Journal*, 233, 159–167. DOI: 10.1016/j.cej.2013.08.035.

[2] Nakagawa, Y., Tomishige, K. (2011). Heterogeneous catalysis of the glycerol hydrogenolysis. *Catalysis Science & Technology,* 1, 179–190. DOI: 10.1039/c0cy00054j.

[3] Sudarsanam, P., Mallesham, B., Prasad, A.N., Reddy, P.S., Reddy, B.M. (2013). Synthesis of bio – additive fuels from acetalization of glycerol with benzaldehyde over molybdenum promoted green solid acid catalysts. *Fuel Processing Technology,* 106, 539–545. DOI: 10.1016/j.fuproc.2012.09.025.

[4] Bagnato, G., Iulianelli, A., Sanna, A., Basile, A. (2017). Glycerol Production and Transformation: A Critical Review with Particular Emphasis on Glycerol Reforming Reaction for Producing Hydrogen in Conventional and Membrane Reactors. *Membranes*, 7(2), 1–17. DOI: 10.3390/membranes7020017.

[5] Christy, S., Noschese, A., Lomelí-Rodriguez, M., Greeves, N., Lopez-Sanchez, J.A. (2018). Recent progress in the synthesis and applications of glycerol carbonate. *Current Opinion in Green and Sustainable Chemistry,* 14, 99–107. DOI: 10.1016/j.cogsc.2018.09.003.

[6] Katryniok, B., Dumeignil, F. (2013). Recent developments in the field of catalytic dehydration of glycerol to acrolein. *ACS Catalysis*, 3, 1819–1834. DOI: 10.1021/cs400354p.

[7] Cornejo, A., Barrio, I., Campoy, M., Lázaro, J., Navarrete, B. (2017). Oxygenated fuel additives from glycerol valorization. Main production pathways and effects on fuel properties and engine performance: A critical review. *Renewable and Sustainable Energy Reviews,* 79, 1400–1413. DOI: 10.1016/j.rser.2017.04.005.

[8] Silva, C.X.A., Gonçalves, V.L.C., Mota, C.J.A. (2009). Water-tolerant zeolite catalyst for the acetalisation of glycerol. *Green Chemistry*, 11(1), 38–41. DOI: 10.1039/b813564a.

[9] Rahmat, N., Abdullah, A.Z., Mohamed, A.R. (2010). Recent progress on innovative and potential technologies for glycerol transformation into fuel additives: A critical review. *Renewable and Sustainable Energy Reviews,* 14, 987–1000. DOI:10.1016/j.rser.2009.11.010.

[10] Pham, T.T., Crossley, S.P., Sooknoi, T., Lobban, L.L., Resasco, D.E., Mallinson, R.G. (2010). Etherification of aldehydes, alcohols and their mixtures on Pd / SiO$_2$ catalysts. *Applied Catalysis A, General,* 379(1–2), 135–140. DOI: 10.1016/j.apcata.2010.03.014.

[11] Gu, Y., Azzouzi, A., Pouilloux, Y. (2008). Heterogeneously catalyzed etherification of glycerol: new pathways for transformation of glycerol to more valuable chemicals. *Green Chemistry*, 10, 164–167. DOI: 10.1039/b715802e.

[12] Silva, C.R.B., Gonçalves, V.L.C., Lachter, E.R., Mota, C.J.A. (2009). Etherification of Glycerol with Benzyl Alcohol Catalyzed by Solid Acids. *Journal of the Brazilian Chemical Society,* 20(2), 201–204. DOI: 10.1590/S0103-50532009000200002.

[13] Gupta, M., Kumar, N. (2012). Scope and opportunities of using glycerol as an energy source. *Renewable and Sustainable Energy Reviews*, 16(7), 4551–4556. DOI: 10.1016/j.rser.2012.04.001.

[14] Sun, D., Yamada, Y., Sato, S., Ueda, W. (2016). Glycerol hydrogenolysis into useful C3 chemicals. *Applied Catalysis B: Environmental*, 193, 75–92. DOI: 10.1016/j.apcatb.2016.04.013.

[15] Yamamoto, K., Kiyan, A.M., Bagio, J.C., Rossi, K.A.B., Delabio Berezuk, F., Berezuk, M.E. (2019). Green cyclic acetals production by glycerol etherification reaction with benzaldehyde using cationic acidic resin. *Green Processing and Synthesis*, 8(1), 183-190. DOI: 10.1515/gps-2018-0059.

[16] Khayoon, M.S., Hameed, B.H. (2011). Acetylation of glycerol to biofuel additives over sulfated activated carbon catalyst. *Bioresource Technology,* 102(19), 9229–9235. DOI: 10.1016/j.biortech.2011.07.035.

[17] Gonçalves, M., Rodrigues, R., Galhardo, T.S., Carvalho, W.A. (2016). Highly selective acetalization of glycerol with acetone to solketal over acidic carbon-based catalysts from biodiesel waste. *Fuel*, 181, 46–54. DOI: 10.1016/j.fuel.2016.04.083.

[18] Ekinci, E.K., Oktar, N. (2019). Production of value-added chemicals from esterification of waste glycerol over MCM-41 supported catalysts. *Green Processing and Synthesis,* 8(1), 128–134. DOI: 10.1515/gps-2018-0034.

[19] De Canck, E., Dosuna-Rodríguez, I., Gaigneaux, E.M., Van Der Voort, P. (2013). Periodic mesoporous organosilica functionalized with sulfonic acid groups as acid catalyst for glycerol acetylation. *Materials*, 6(8), 3556–3570. DOI: 10.3390/ma6083556.

[20] Sánchez, J.A., Hernández, D.L., Moreno, J.A., Mondragón, F., Fernández, J.J. (2011). Alternative carbon based acid catalyst for selective esterification of glycerol to acetylglycerols. *Applied Catalysis A: General,* 405(1–2), 55–60. DOI: 10.1016/j.apcata.2011.07.027.

[21] Gonzalez-Arellano, C., De, S., Luque, R. (2014). Selective glycerol transformations to high value-added products catalysed by aluminosilicate-supported iron oxide nanoparticles. *Catalysis Science and Technology*, 4(12), 4242–4249. DOI: 10.1039/c4cy00714j.

[22] Khayoon, M.S., Triwahyono, S., Hameed, B.H., Jalil, A.A. (2014). Improved production of fuel oxygenates via glycerol acetylation with acetic acid. *Chemical Engineering Journal*, 243, 473–484. DOI: 10.1016/j.cej.2014.01.027.

[23] Gonçalves, C.E., Laier, L.O., Cardoso, A.L., José, M. (2012). Bioadditive synthesis from $H_3PW_{12}O_{40}$-catalyzed glycerol esterification with HOAc under mild reaction conditions. *Fuel Processing Technology,* 102, 46–52. DOI: 10.1016/j.fuproc.2012.04.027.

[24] Wang, L., Liu, Q., Zhou, M., Xiao, G. (2012). Synthesis of glycerin triacetate over molding zirconia-loaded sulfuric acid catalyst. *Journal of Natural Gas Chemistry,* 21(1), 25–28. DOI: 10.1016/S1003-9953(11)60328-9.

[25] Zhu, S., Zhu, Y., Gao, X., Mo, T., Zhu, Y., Li, Y. (2013). Production of bioadditives from glycerol esterification over zirconia supported heteropolyacids. *Bioresource Technology,* 130, 45–51. DOI: 10.1016/j.biortech.2012.12.011.

[26] Dhakshinamoorthy, A., Alvaro, M., Garcia, H. (2012). Commercial metal–organic frameworks as heterogeneous catalysts. *Chemical Communications*, 48(92), 11275–11288. DOI: 10.1039/c2cc34329k.

[27] Zhou, C.H., Beltramini, J.N., Lu, G.Q. (2008). Chemoselective catalytic conversion of glycerol as a biorenewable source to valuable commodity chemicals. *Chemical Society Reviews,* 37(3), 527–549. DOI: 10.1039/b707343g.

[28] Trifoi, A.R., Agachi, P.Ş., Pap, T. (2016). Glycerol acetals and ketals as possible diesel additives. A review of their synthesis protocols. *Renewable and Sustainable Energy Reviews*, 62, 804–814. DOI: 10.1016/j.rser.2016.05.013.

[29] Cai, Q., Lin, W.Y., Xiao, F.S., Pang, W.Q., Chen, X.H., Zou, B.S. (1999). The preparation of highly ordered MCM-41 with extremely low surfactant concentration. *Microporous and Mesoporous Materials*, 32(1–2), 1–15. DOI: 10.1016/S1387-1811(99)00082-7.

[30] Corma, A., Fornés, V., Navarro, M.T., Pérez-Pariente, J. (1994). Acidity and stability of MCM-41 crystalline aluminosilicates. *Journal of Catalysis,* 148(2), 569–574. DOI: 10.1006/jcat.1994.1243.

[31] Heravi, M.M., Hosseini, M., Oskooie, H.A., Baghernejad, B. (2011). Fe/Al-MCM-41: An efficient and reusable catalyst for the synthesis of quinoxaline derivatives. *Journal of the Korean Chemical Society,* 55(2), 235–239. DOI: 10.5012/jkcs.2011.55.2.235.

[32] Oprescu, E.E., Stepan, E., Dragomir, R.E., Radu, A., Rosca, P. (2013). Synthesis and testing of glycerol ketals as components for diesel fuel. *Fuel Processing Technology,* 110, 214–217. DOI: 10.1016/j.fuproc.2012.12.017.

[33] Kim, I., Kim, J., Lee, D. (2014). A comparative study on catalytic properties of solid acid catalysts for glycerol acetylation at low temperatures. *Applied Catalysis B: Environmental*, 148–149, 295–303. DOI: 10.1016/j.apcatb.2013.11.008.

[34] Mallesham, B., Govinda Rao, B., Reddy, B.M. (2016). Production of biofuel additives by esterification and acetalization of bioglycerol. *Comptes Rendus Chimie*, 19(10), 1194–1202. DOI: 10.1016/j.crci.2015.09.011.

[35] Li, X., Zheng, L., Hou, Z. (2018). Acetalization of glycerol with acetone over $Co[II](Co[III]xA_{l2-x})O_4$ derived from layered double hydroxide. *Fuel*, 233, 565–571. DOI: 10.1016/j.fuel.2018.06.096.

[36] Zhang, S., Zhao, Z., Ao, Y. (2015). Design of highly efficient Zn-, Cu-, Ni- and Co-promoted M-AlPO$_4$ solid acids: The acetalization of glycerol with acetone. *Applied Catalysis A: General*, 496, 32–39. DOI: 10.1016/j.apcata.2015.02.006.

[37] Schuette, H.A., Hale, J.T. (1930). Some physical constants of monacetin, monopropin and mono-normal-butyrin. *Journal of the American Chemical Society,* 52(5), 1978–1981. DOI: 10.1021/ja01368a033.

[38] Gilchrist, P.G., Schuette, H.A. (1931). Monoglycerides of the lower fatty acids. *Journal of the American Chemical Society,* 53(9), 3480–3484. DOI: 10.1021/ja01360a038.

[39] Cho, G.H.P., Yeong, S.K., Ooi, T.L., Chuah, C.H. (2006). Glycerol esters from the reaction of glycerol with dicarboxylic acid esters. *Journal of Surfactants and Detergents*, 9(2), 147–152. DOI: 10.1007/s11743-006-0384-9.

[40] Rathod, A.P., Wasewar, K.L., Sonawane, S.S. (2014). Enhancement of esterification of propionic acid with ethanol by pervaporation reactor. *Research Journal of Chemistry and Environment*, 18(5), 41–44. DOI: 10.1155/2014/539341.

[41] Saengarun, C., Petsom, A., Tungasmita, D.N. (2017). Etherification of glycerol with propylene or 1-butene for fuel additives. *Scientific World Journal*, 2017, 1-11. DOI: 10.1155/2017/4089036.

[42] Preethi, E.L., Revathi, S., Sivakumar, T., Manikandan, D., Divakar, D., Valentine-Rupa, A., Palanichami, M. (2008). Phenol hydroxylation using Fe/Al-MCM-41 catalysts. *Catalysis Letters*, 120(1–2), 56–64. DOI: 10.1007/s10562-007-9249-8.

[43] Decyk, P., Trejda, M., Ziolek, M., Kujawa, J., Głaszczka, K., Bettahar, M., Monteverdi, S., Mercy, M. (2003). Physicochemical and catalytic properties of iron-doped silica - The effect of preparation and pretreatment methods. *Journal of Catalysis,* 219(1), 146–155. DOI: 10.1016/S0021-9517(03)00186-6.

[44] Missen, R.W., Mims, C.A., Saville, B.A. (1999). *Introduction to Chemical Reaction Engineering and Kinetics*, New York, John Wiley & Sons.

[45] Silva, C., Mota, C.J.A., Pinto, B.P. (2008). Acetylation of glycerol catalyzed by different solid acids. *Catalysis Today,* 133-135, 673–677. DOI: 10.1016/j.cattod.2007.12.037.

[46] Beck, J.S., Vartuli, J.C., Roth, W.J., Leonowicz, M.E., Kresge, C.T., Schmitt, K.D., Chu, C.T.W., Olson, D.H., Sheppard, E.W., McCullen, S.B., Higgins, J.B., Schlenker, J.L. (1992). A New Family of Mesoporous Molecular Sieves Prepared with Liquid Crystal Templates. *Journal of the American Chemical Society,* 114(27), 10834–10843. DOI: 10.1021/ja00053a020.

[47] Ajaikumar, S., Pandurangan, A. (2008). Reaction of benzaldehyde with various aliphatic glycols in the presence of hydrophobic Al-MCM-41: A convenient synthesis of cyclic acetals. *Journal of Molecular Catalysis A: Chemical*, 290(1–2), 35–43. DOI: 10.1016/j.molcata.2008.04.008.

[48] Mate, V.R., Shirai, M., Rode, C.V. (2013). Heterogeneous Co$_3$O$_4$ catalyst for selective oxidation of aqueous veratryl alcohol using molecular oxygen. *Catalysis Communications*, 33(3), 66–69. DOI: 10.1016/j.catcom.2012.12.015.

[49] Abdelkader, A., Daly, H., Saih, Y., Morgan, K., Mohamed, M.A., Halawy, S.A., Hardacre, C. (2013). Steam reforming of ethanol over Co$_3$O$_4$-Fe$_2$O$_3$ mixed oxides. *International Journal of Hydrogen Energy*, 38(20), 8263–8275. DOI: 10.1016/j.ijhydene.2013.04.009.

[50] Alves, I.C.B., Santos, J.R.N., Viégas, D.S.S., Marques, E.P., Lacerda, C.A., Zhang, L., Zhang, J., Marques, A.L.B. (2019). Nanoparticles of Fe$_2$O$_3$ and Co$_3$O$_4$ as efficient electrocatalysts for oxygen reduction reaction in acid medium. *Journal of the Brazilian Chemical Society*, 30(12), 2681–2690. DOI: 10.21577/0103-5053.20190195.

[51] Ertl, G., Knözinger, H., Schülf, F, Weitkamp, J. (1997). *Handbook of Heterogeneous Catalysis*, Germany, Wiley-VCH.

[52] Fontes, M.S.B., Melo, D.M.A., Costa, C.C., Melo, M.A.F., Alvez, J.A.B.L.R., Silva, M.L.P. (2016). Effect of different silica sources on textural parameters of molecular sieve MCM-41. *Ceramica,* 62, 85-90. DOI: 10.1590/0366-69132016623611966.

[53] Selvaraj, M., Pandurangan, A., Seshadri, K.S., Sinha, P.K., Lal, K.B. (2003). Synthesis, characterization and catalytic application of MCM-41 mesoporous molecular sieves containing Zn and Al. *Applied Catalysis A: General*, i(2), 347–364. DOI: 10.1016/S0926-860X(02)00527-6.

[54] Camblor, M.A., Corma, A., Pérez-Pariente, J. (1993). Infrared spectroscopic investigation of titanium in zeolites. A new assignment of the 960 cm^{-1} band. *Journal of the Chemical Society, Chemical Communications*, 6, 557–559. DOI: 10.1039/C39930000557.

[55] Vidya, K., Gupta, N.M., Selvam, P. (2004). Influence of pH on the sorption behaviour of uranyl ions in mesoporous MCM-41 and MCM-48 molecular sieves. *Materials Research Bulletin*, 39(13), 2035–2048. Doi: 10.1016/j.materresbull.2004.07.013.

[56] Alves, I.C.B., Santos, J.R.N., Viégas, D.S.S., Marques, E.P., Lacerda, C.A., Zhang, L., Zhang, J, Marques, A.L.B. (2019). Nanoparticles of Fe_2O_3 and Co_3O_4 as efficient electrocatalysts for oxygen reduction reaction in acid medium. *Journal of the Brazilian Chemical Society,* 30, 2681-2690. DOI: 10.21577/0103-5053.20190195.

[57] Sahoo, S., Agarwal, K., Singh, A., Polke, B., Raha, K. (2011). Characterization of g- and α-Fe_2O_3 nano powders synthesized by emulsion precipitation-calcination route and rheological behaviour of α-Fe_2O_3. *International Journal of Engineering, Science and Technology*, 2(8), 118–126. DOI: 10.4314/ijest.v2i8.63841.

[58] Varghese, S., Cutrufello, M.G., Rombi, E., Cannas, C., Monaci, R., Ferino, I. (2012). CO oxidation and preferential oxidation of CO in the presence of hydrogen over SBA-15-templated CuO-Co_3O_4 catalysts. *Applied Catalysis A: General*, 443–444, 161–170. DOI: 10.1016/j.apcata.2012.07.038.

[59] Borade, R.B., Clearfield, A. (1995). Synthesis of aluminum rich MCM-41. *Catalysis Letters*, 31(2–3), 267–272. DOI: 10.1007/BF00808839.

[60] Savidha, R, Pandurangan, A. (2004) Isopropylation of toluene: a comparative study of microporous zeolites and mesoporous MCM-41 materials. *Applied Catalysis A: General*, 276, 39–50. DOI: 10.1016/j.apcata.2004.04.015.

[61] Carmo Jr, A.C., Souza, L.K.C., Costa, C.E.F., Longo, E., Zamina, J.R., Rocha-Filho, G.N. (2009) Production of biodiesel by esterification of palmitic acid over mesoporous aluminosilicate Al-MCM-41. *Fuel*, 88, 461-468. DOI: 10.1016/j.fuel.2008.10.007.

[62] Samanta, S., Giri, S., Sastry, P.U., Mal, N.K., Manna, A., Bhaumik, A. (2003). Synthesis and characterization of iron-rich highly ordered mesoporous Fe-MCM-41. *Industrial and Engineering Chemistry Research*, 42(13), 3012–3018. DOI: 10.1021/ie020905g.

[63] Tran, N.T.T., Uemura, Y., Ramli, A. (2016). Hydrodeoxygenation of Guaiacol over Al-MCM-41 Supported Metal Catalysts: A Comparative Study of Co and Ni. *Procedia Engineering*, 148, 1252–1258. DOI: 10.1016/j.proeng.2016.06.488.

[64] Udayakumar, S., Ajaikumar, S., Pandurangan, A. (2006). Synthesis of commercial important diethyl phthalate over Al-, Fe- and Al, Zn-MCM-41 molecular sieves. *Applied Catalysis A: General*, 307(2), 245–256. DOI: 10.1016/j.apcata.2006.03.059.

[65] Fletcher, R.E., Ling, S., Slater, B. (2017). Violations of Löwenstein's rule in zeolites. *Chemical Science*, 8(11), 7483–7491. DOI: 10.1039/c7sc02531a.

[66] Uytterhoeven, J.B., Christner, L.G., Hall, W.K. (1965). Studies of the hydrogen held by solids. VIII. The decationated zeolites. *Journal of Physical Chemistry*, 69(6), 2117–2126. DOI: 10.1021/j100890a052.

[67] Pearson, R.G. (1963). Hard and Soft Acids and Bases. *Journal of the American Chemical Society*, 85(22), 3533–3539. DOI: 10.1021/ja00905a001.

[68] Vasconcellos, M.L.A.A. (2014) A Teoria de Pearson para a disciplina de química orgânica: um exercício prático e teórico aplicado em sala de aula. *Química Nova*, 37, 171–175. DOI: 10.1590/S0100-40422014000100029.